Design and Development of an Active Magnetic Docking System for Small Satellites

Atheel Redah, Saurav Paudel, Milan Pathak, Chaitanya Athawle, Om Sai Swaroop Mopidevi, Felix Sittner, Sergio Montenegro
Chair of Aerospace Information Technology, University of Wuerzburg
Emil-Fischer-Strasse 70, 97074 Wuerzburg, Germany; +49-931-31-83974
atheel.redah@uni-wuerzburg.de

ABSTRACT

Applications such as self-assembly and reconfiguration in space, on-orbit servicing and refueling, debris and retired elements removal are examples of future space missions that will require space objects that can perform autonomous rendezvous and docking maneuvers with other orbiting elements.

To demonstrate such capability for small satellites, the TAMARIW project is intended to develop two identical 3U CubeSats with autonomous docking systems. These satellites are scheduled to be launched by the end of the first quarter of 2026 to perform several undocking/docking maneuvers in space at predefined relative distances. In addition, the standardization and partial autonomy of the satellite modules will be tested. In case of a failure detected in one satellite, a Recovery and Takeover Protocol can be initiated. In this protocol, the other satellite can send commands to the actuators and receive sensors information directly from the recovered satellite over wireless connection.

Developing an autonomous docking system for small satellites that can guarantee safe automated docking process is very challenging. Small satellites have strict limitations in mass and volume which result in limited power and maneuvering capability. Also, the limited volume restricts the use of complex mechanisms for berthing and docking operations. Magnetic docking systems provides a very good solution to overcome these problems since it can help in both capturing and alignment process to perform close range docking maneuvers without the need of using the propulsion system of the satellite which is difficult to utilize in close proximity. One important problem with using such a system is the effect of the disturbance torque that can generate due to the interaction of the magnetic field of the docking system with the magnetic field of the Earth. Furthermore, the heat dissipation problem needs to be thoroughly analyzed.

This paper will describe the magnetic docking module being developed. The mechanical and electrical designs of the active magnetic docking system will be explained. The latching mechanisms intended to be developed and tested will be outlined. The guidance and docking control subsystem and the docking control strategy being developed will be described. Additionally, a thermal analysis of the guidance and docking control subsystem will be presented.

INTRODUCTION

The rapidly increased number of small satellites orbiting the earth mainly for communication and observation purposes will require in the near future an increase demands for these satellites to be able to perform autonomous docking maneuvers to extend the life or functionalities of nearby satellites or even to lower the orbit of out of service satellites. This will require a very reliable autonomous docking system that can guarantee a safe docking process and with simplified design to be able to integrate it into the satellites easily.

The active magnetic docking system being developed in the TAMARIW "TeilAutonome Montage/Aufbau und Rekonfiguration Im Weltraum" project is an innovative approach to develop and demonstrate such capability for small satellites. In this approach, the satellites should be able to perform several autonomous undocking/docking maneuvers at predefined relative distances using an onboard guidance and docking control subsystem. After docking, the satellites should act together, for example their attitude control and orbital maneuvers will be coordinated and executed synchronously as if they were a single unit. In addition, an out of service satellite can be recovered after docking by initiating a developed Recovery and Takeover Protocol to change its orientation, adjust its orbit, upgrade its software or even perform an end-of-life maneuver.

MECHANICAL DESIGN

The mechanical design of the developed active magnetic docking system consists mainly of four electromagnets placed at the corners of one side of the CubeSat defined as the docking side. These four electromagnets will ensure a very good alignment for the satellite with the other satellite during docking process as the force exerted on the satellite corners due to the magnetic field will be fully controllable.

Initially, electromagnetic cores with a circular cross-section were designed and developed. However, during testing, it was observed that the satellites often experienced disorientation and failed to dock as expected. To address this issue, a new design for the electromagnetic cores was proposed and tested. This design, which features Probe and Drogue cores, has shown promise in achieving perfect alignment for the satellites. During the tests, this design consistently yielded excellent docking results. The design is shown in Figures 1.
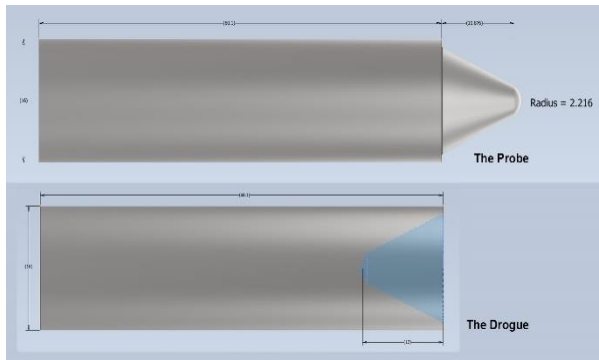

Figure 1: The Probe and Drogue Design of The Electromagnets

The new probe-drogue design offers several significant benefits. During the attraction phase, the probe profile exhibits a higher magnetic flux density compared to the previous cylindrical core design. This is because of the extended tip of the probe. When the probe and drogue are brought within a predetermined docking distance, the attraction force ensures they come into contact. The probe tip, with its higher magnetic flux density, is strongly drawn into the drogue's inner section. The drogue's shape then helps align the probe's central axis with its own. The drogue's shape creates a magnetic loop around its outer ring, resulting in a higher magnetic flux density at this ring than at the center. As the probe is drawn into this loop, the magnetic flux assists in achieving better alignment for docking.

The variation in magnetic force relative to the distance between two electromagnets is illustrated in Figure 2.
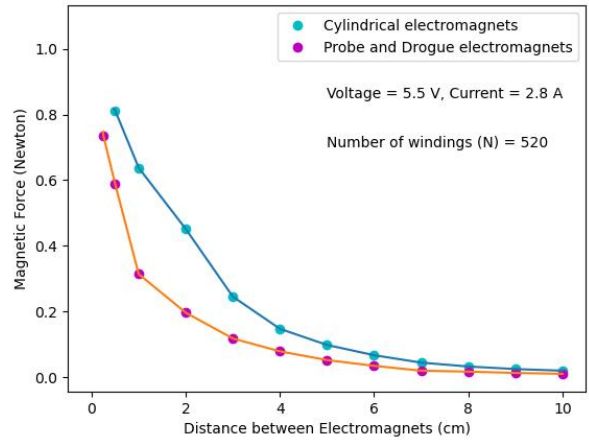

Figure 2: The Variation in Magnetic Force Relative to the Distance between Two Electromagnets

From the above graph, we can observe that the previous cylindrical design has slightly stronger attraction force for the same distance. This implies that the cylindrical core generates stronger force compared to the probe and drogue configuration. However, probe and drogue configuration demonstrates perfect alignment for docking which is a requirement for the proper operation of the latching mechanism.

The electromagnetic simulation for the probe and drogue configuration at a relative distance of 20 cm can be shown in Figure 3.
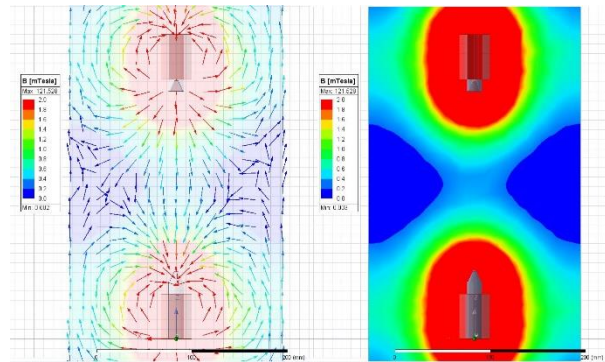

Figure 3: The Electromagnetic Simulation of the Probe and Drogue Configuration

The final version of the developed electromagnets has coil of approximately 600 turns with diameter of 32 mm and length of 46 mm. The ferromagnetic cores of the electromagnets are made from Invar 36 (nickel-iron alloy) which displays high dimensional stability over a range of temperatures.

To house and protect the electromagnets and the battery assembly used to power the docking system, a casing unit that holds two electromagnets (probe-and-drogue)

and battery back consisting of two batteries has been designed and developed. The casing unit ensures proper functioning of these components by providing mechanical and thermal isolation from external environment while also aiding in the radiation shielding and thermal performance of the system (heat dissipation from coils and battery). The casing is a two-part assembly consisting of a casing body and cover. This configuration was chosen to efficiently absorb the impact from docking and latching maneuver and transfer it to structural parts of the satellite. Another advantage is ease of alignment and assembly of the electromagnets. The overall size of the casing is 66x91x50 mm and weighs approximately 160 grams. Aluminium 6061-T6 (tempered aluminium alloy) has been used for the casing. The properties of Al6061 make it an excellent choice for this application due to its good strengths to weight ratio as well as mechanical strength. Secondly, Al6061 is non-magnetic and has good corrosion resistance, thermal conductivity and machinability.[3] Each satellite will have two of these Electromagnetic Docking Units (EDU) assembled.
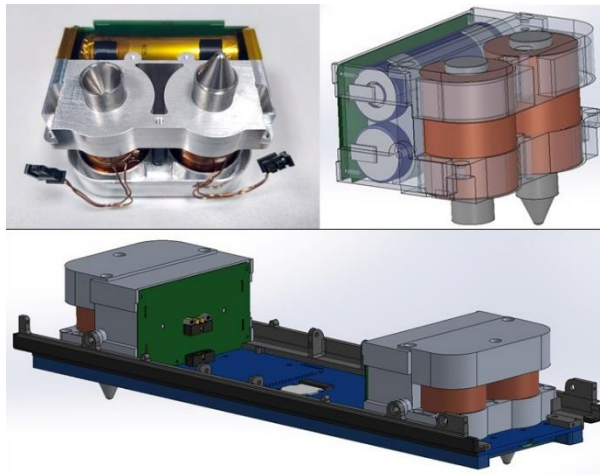

Figure 4: The Electromagnetic Docking Units Assembly

The casing base is attached to the rails on the docking side of the satellite at four mounting points using fasteners. The base is directly attached to the rails for better force transfer to the structural assembly. The battery assembly is also attached to the casing at four mounting points using fasteners. Finally, the cover is fixed to the base using three mounting points using fasteners which locks the electromagnets in place as shown in Figure 4.

LATCHING MECHANISM

A latching mechanism in satellites is a critical component designed to secure and release satellite modules or payloads during various phases of a mission. This mechanism ensures stability and structural integrity during launch, deployment, and operation in space. It consists of mechanical locks, actuators, and sensors that work in a controlled loop to engage and disengage with precision. Latching mechanisms are designed to withstand harsh space conditions, such as extreme temperatures and radiation, while minimizing vibration and shock impacts. Their reliability is crucial for successful satellite deployment, docking procedures, and modular reconfigurations in orbit, thereby enhancing mission versatility and longevity.

In the current application four sets of electromagnets are attached on both satellites with a probe-drogue type configuration for the purpose of final alignment and approach. The electromagnetic interaction brings the alignment of the mating axes withing a tolerance of ±30 degree and controls the approach velocity just enough to overcome the static stiffness of the latching mechanism while achieving a soft docking. Based on the specifications of this application, the latching mechanism must be compact, with the least number of active parts and actuators, isolated from the background electromagnetism, external thermal conditions and radiation. The selection of material for the active components of the mechanism is the most critical part and dictates over the material selection of non-structural non-functional parts. The factors to be considered would be redundancy, thermal expansion, friction and wear at contact points, non-magnetic behavior, ease of manufacturing preferably using additive manufacturing techniques, sufficient yield strength, fatigue and corrosion resistance. Some modern alloys such as titanium, BeCu, or Hastealloy comply to these harsh conditions of space while providing good mechanical strength and fatigue resistance.[4-6] These are being used in various space related applications and can be proposed for this specific application. Redundancy for mechanical components in space is crucial for ensuring the reliability and longevity of space missions. Redundancy involves incorporating backup systems or components that can take over if the primary system fails. This approach is essential given the inability to perform in-person repairs and the harsh conditions of the space environment. Hence the Latching mechanisms must be designed compact and sturdy, to comply with a minimum of dual-redundancy (two-fault tolerant system).

Considering the above constraints, two designs are being developed for the latching process. The first design is Leaf-Spring latch mechanism. Compliant mechanisms are solid body components which make careful use of flexibility of the material and part

geometry to achieve desired motion while avoiding use of mechanical joints. Thus, compliant mechanism can avoid backlash, wear and friction while significantly reducing the number of working parts as compared to conventional equivalent mechanism.[4,7] Further, the Leaf- Spring concept is also used as it provides considerable stiffness for the latch while being simple in design. The combined mechanism is compact and reliable because of the lower number of active parts.

The main part in the latching mechanism is the tri-branch leaf spring (configuration similar to the symbol '∆' joined at the ends with rounded lobes) with the drogue type mating part integrated into it. The drogue cup is divided into three parts which are each supported by a branch of leaf spring. The leaf spring also applies spring force on the drogue cup to keep it closed in static condition. Along with the actuator, it is the only active moving part in the assembly. The guides and tracks for the leaf spring are machined into the top cover of the structure and the casing support is fastened from bottom of assembly to keep leaf spring in place and to fasten the actuators.
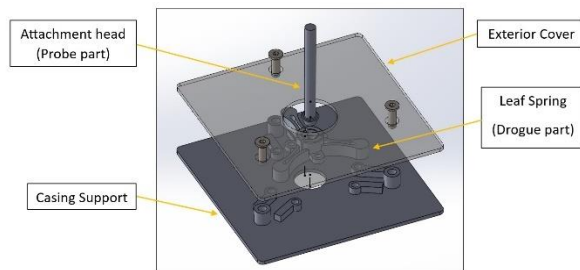

Figure 5: Leaf-Spring Latch Mechanism

The leaf spring mechanism is a mono-stable dual state mechanism and operates in the 'Locked' and 'Unlocked' states. The mechanism is naturally statically stable only in the 'Locked' condition due to the compressive force of the leaf springs. The mechanism can then be switched to and held at the 'Unlocked' condition using the actuator pull force acting against the leaf springs.

The entry part of the drogue is tapered inwards for controlled engagement, i.e. to correct for small degrees of axial misalignment and guides the probe to make proper contact. It also improves the conversion of impulse forces by the probe to potential energy helping in expansion the leaf spring. During initial contact and docking, the probe (attachment head) transfers the momentum of the docked satellite to the latching mechanism through the tapered surface of the drogue part. This impulse force is then stored in form of potential energy by the leaf springs which pushes it

outwards. This outward motion of the leaf spring opens the drogue cup, allowing the probe to travel past the tapered surface. The mechanism shifts from 'Locked state' to 'Unlocked state' and is held in this state till the probe clears the tapered portion. Once the probe has cleared the tapered section, spring tension causes the drogue cup to close back to its initial 'Locked' state. This locks the probe into the drogue. Further, the rear part of the drogue has an inverted taper which matches with inverted taper on the probe part which creates self-locking force on the drogue part. This ensures positive lock of the drogue in case of small disturbance forces or vibrations.
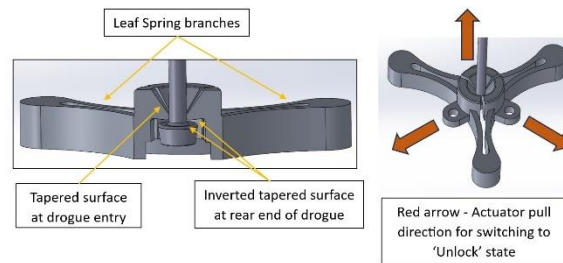

Figure 6: Leaf-Spring Latching Mechanism Operation

The second design is Ball-Lock latch mechanism. Ball-Lock mechanisms are commonly used in various aerospace applications due to their reliability, simplicity, and strong holding capability. It also performs well in vibrations and shock environment with large holding loads.[8-10]
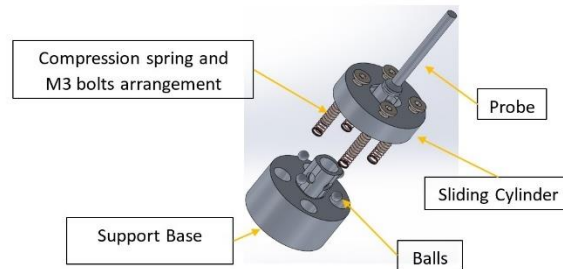

Figure 7: Ball-Lock Latch Mechanism

Ball lock mechanism is a mono-stable dual state mechanism and operates in the 'Locked' and 'Unlocked' states. The mechanism is naturally statically stable only in the 'Locked' condition due to the preload of the compression springs. The mechanism can then be switched to and held at the 'Unlocked' condition using the actuator pull force acting against the compression springs.

During the 'Locked' condition, the sliding cylinder is at its top-most position and presses the balls into the

grooves of the support base. The design of the cavity is such that when the balls are pressed into the cavity, some surface of the ball protrudes into the latching bore which blocks the path of the probe. The mechanism is switched to the 'Unlocked' by pulling the sliding cylinder to its lowest travel position using an actuator. The internal groove geometry of the sliding cylinder is designed to allow the ball to retract into the cavity just enough that no surface of the ball is protruding into the latching bore. This creates an unrestricted path for the probe to enter/exit the latching bore. Hence, it's essential to bring the mechanism in 'Unlocked' condition for docking and undocking procedure. The sequence for docking procedure is illustrated in Figure 8.
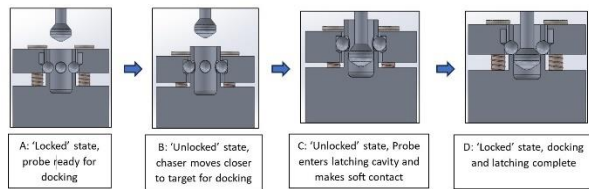

Figure 8: The Sequence for Docking Procedure for the Ball-Lock Latch Mechanism

Since the mechanism is bought to the 'Unlocked' stated before Docking and Undocking, the sequence for Undocking procedure is like the Docking procedure but in reverse order.

ELECTRICAL DESIGN

The electrical design of the developed active magnetic docking system consists of a main Printed Circuit Board (PCB) for the Guidance and Docking Control (GDC) subsystem and a power subsystem.
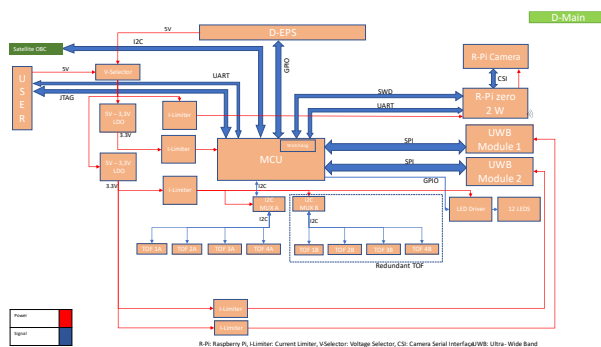

Figure 9: The Block Diagram of the Guidance and Docking Control Subsystem

Figure 9 contains the block diagram of the GDC subsystem. The system consists of an STM32F4 ARM Cortex M4-based high-performance 32-bit microcontroller, a Raspberry Pi Zero 2W ARM Cortex

A53-based 64-bit single-board computer clocked at 1GHz, eight Time-of-Flight (ToF) proximity sensors, two Ultra-Wideband (UWB) modules, camera, 12 LEDs and current limiters for these electronic components. The GDC microcontroller communicates with satellite main On-Board Computer (OBC) via I2C bus. The microcontroller can be programmed either wirelessly through the Serial Wire Debug (SWD) pins of the Raspberry Pi or via the JTAG pins using the EGSE (Electronic Ground Support Equipment). The operator can also communicate with the GDC subsystem via EGSE and can also power the system for the debugging purposes before launch. The GDC subsystem has two I2C multiplexers connected to two sets of four ToF sensors in which one set acts as a redundant unit. The microcontroller is connected to two UWB modules and communicates over SPI. The Raspberry Pi is connected to the microcontroller over UART and SWD. The UART connection is used to share the information between the microcontroller and the Raspberry Pi and the SWD pins are used to program the microcontroller wirelessly. The camera is also connected to the Raspberry Pi over the Camera Serial Interface (CSI) pins. The GDC also contains 12 LEDS which are independently controlled by the GPIOs of the microcontroller via a LED Driver. All the main units are protected by a current limiter and the setpoint of the current limit can be set based on the consumption of the units.

The power for all these units is provided by the active magnetic docking power subsystem which is explained using the block diagram shown in Figure 10.
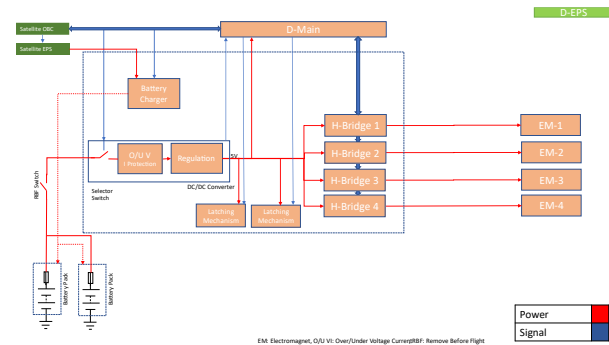

Figure 10: The Block Diagram of the Active Magnetic Docking Power Subsystem

The power is provided by two battery packs which are connected in parallel. Each battery pack contains two Lithium-Ion batteries of 3.6 V and 4000 mAh capacity connected in series making the total configuration for the battery in the docking system to 7.2 V / 8000 mAh / 2S2P. Each battery pack also has a fuse for short circuit protection. The battery is connected to the DC-DC

converter via a remove-before-switch and a controllable switch. The controllable switch turns off the power of the system and is controlled by the input from the main OBC of the satellite. Therefore, the docking system is powered off until the docking phase arises and only the main OBC can enable it. The satellite main Electrical Power System (EPS) can also charge the batteries of the active magnetic docking power subsystem. The system is protected by under and overvoltage protection of the DC-DC converter. The output of the DC-DC converter is set to 5.5 V which is the operating BUS voltage of the docking system. Each electromagnet will be H-bridge driven and controlled through Pulse-width Modulation (PWM) and direction signals provided by the microcontroller to have dual polarity electromagnet with controlled magnetic field strength. The maximum voltage input provided to these electromagnets is 5.5 V. The docking system also contains two latching mechanisms controller and the power supplied to these latching mechanisms is also from the output of the DC-DC converter. The latching mechanism electronics is based on the MOSFET based electronic switch controlled by the microcontroller.
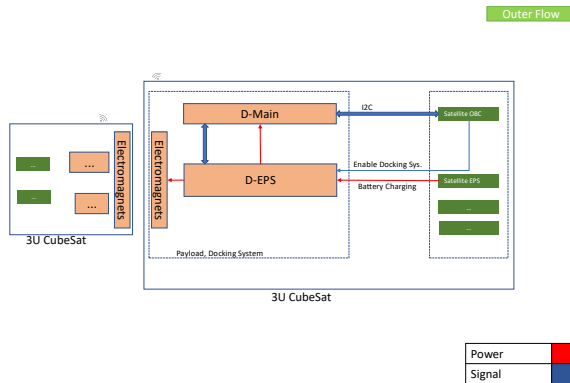

Figure 11: The Block Diagram of the Two 3U CubeSats

Figure 11 shows the block diagram of the two 3U CubeSats containing these above-mentioned units in the docking system which is the payload of the satellite. The two satellites communicate wirelessly with each other.

THE GUIDANCE AND DOCKING CONTROL SUBSYSTEM

Performing safe and successful autonomous docking maneuver for CubeSats is a very challenging task. The strict limitations in mass and volume make it very difficult to use complex mechanisms or advanced guidance sensor systems. To overcome this problem and to minimize the risk of failure or operational error, a multistage guidance sensor subsystem has been developed. In this system, the docking side of each satellite will have three stages of sensor systems as shown in Figure 12.
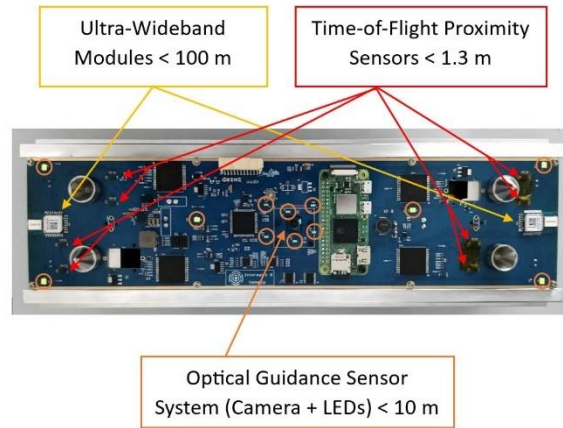

Figure 12: The Guidance and Docking Control Subsystem

The first stage will be using two UWB modules to estimate the relative position of the other satellite for a medium relative distance range less than 100 m. Meanwhile, the second stage will be using an Optical Guidance Sensor System consist of a camera and two sets of LEDs indicators to identify the docking surface and the relative position and orientation of the other satellite for a short relative distance range less than 10 m. Finally, and for the last stage, four ToF proximity sensors are used to indicate the relative distance, velocity, and tilt angles of the other satellite for a very short distance range less than 1300 mm and up to proximity range of 1 mm.

The last stage of sensors estimation is very critical for the overall docking operation. To increase the reliability of the system, a second set of ToF sensors has been added as redundant. As soon as a failure is detected with one set of the ToF sensors. A fault tolerance algorithm will be activated, and the second set of sensors will be utilized. To ensure proper operation and as shown in Figure 12, The ToF sensors has been distributed in a such way that no ToF sensors should face each other while docking.

An Optical Guidance Sensor System that can estimate relative position and orientation of the other satellite and robust against external light sources is developed. The developed algorithm uses a camera to take images at a given interval of a target satellite with LED markers placed in two patterns on the docking side. These images are pre-processed to remove most external light sources and then all bright light sources are tracked. Each LED on the target satellite blinks a specific binary code that allows the system to

distinguish the LEDs on the target satellite from any other light source and determine the LED's corresponding model points on the target satellite model. The sensor then estimates the relative position and orientation of the target satellite using Perspective-n-Point (PnP) algorithm. Two patterns of six LEDs each have been employed as shown in Figure 12. An outer pattern for a short range less than 10 m and up to 100 cm and an inner pattern for a very short range up to 10 cm. The system has been designed to have a fault tolerance capability to maintain proper operation even in case two LEDs are not functioning in a single pattern.

Four UWB modules will be used to estimate the 3D relative positions of the satellites. The system is realized by fusing 3D position estimations from an UWB transceiver network in the two satellites with Inertial Measurement Unit (IMU) sensor data coming from the satellite's Attitude Determination and Control System (ADCS).

The 3D relative position data gathered from stage one and two of the sensor systems will be filtered using Extended Kalman filter algorithm and then forwarded to the satellite's ADCS to be utilized by the rendezvous and attitude control system.

The electromagnets are only activated for Capture and Alignment if other docking surface are in the range of a threshold distance (ca. 40 cm) and both docking sides are aligned with each other in a face-to-face manner with a predefined clearance value of ±30 degree in roll/pitch/yaw. Two modes of operations are implemented for the developed docking system where the electromagnets are set to generate an Attraction/Repulsive force for the corresponding Docking/Undocking operation.

The docking controller will require real-time computing with minimum overhead and fault tolerant capabilities. Therefore, the Real-time Onboard Dependable Operating System (RODOS) will be used. It has Middleware with Topics and Subscribers beside a Gateway that brings Topics to other RODOS nodes. RODOS will be running on the microcontroller and will provide the software framework for running the docking controller and gathering sensors information from stage one and stage three of the guidance sensor subsystem. Stage two will be running on the available Raspberry Pi that also will provide the wireless communication link between the satellites.

Every Satellite will scan its surrounding for targets and possible obstacles using the onboard optical guidance sensor system and at the same time receive Satellite

Status Reports (SSR) from the other satellite using the wireless modules available on the Raspberry Pi single board computers. The SSR will contain information about the satellite position, attitude, and fuel & power remaining capacity.

The GDC subsystem is set to operate in autonomous mode where only main mission commands and sensors information will be exchange between the GDC and the satellite's main OBC to coordinate between the ADCS of the satellite and the GDC subsystem during the rendezvous and docking operation.

Two polarities configurations can be activated depending on the needed conditions for the rendezvous and docking operation, Identical Polarities configuration for the Capturing Phase and Alternating Polarities configuration for the Alignment Phase.

The Identical Polarities configuration is attained by turning the electromagnets in each satellite with the same polarity as shown in Figure 13.
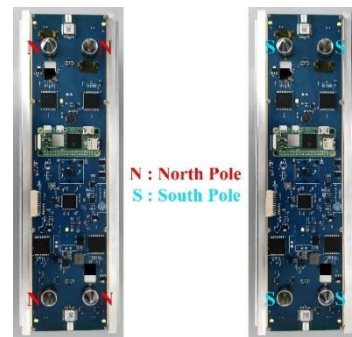

Figure 13: Identical Polarities Configuration (Capturing Phase)

In this configuration, the capturing force between the satellites will be much larger than that of the alternating polarities configuration. The simulation of the magnetic field generated by the eight electromagnets of the two satellites at different relative distances of 10 cm, 20 cm and 30 cm is shown in Figure 15.
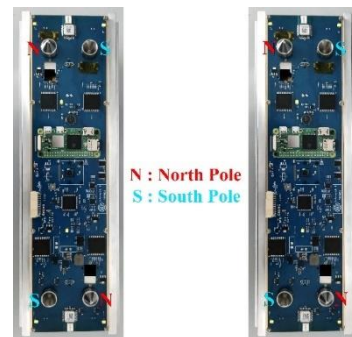

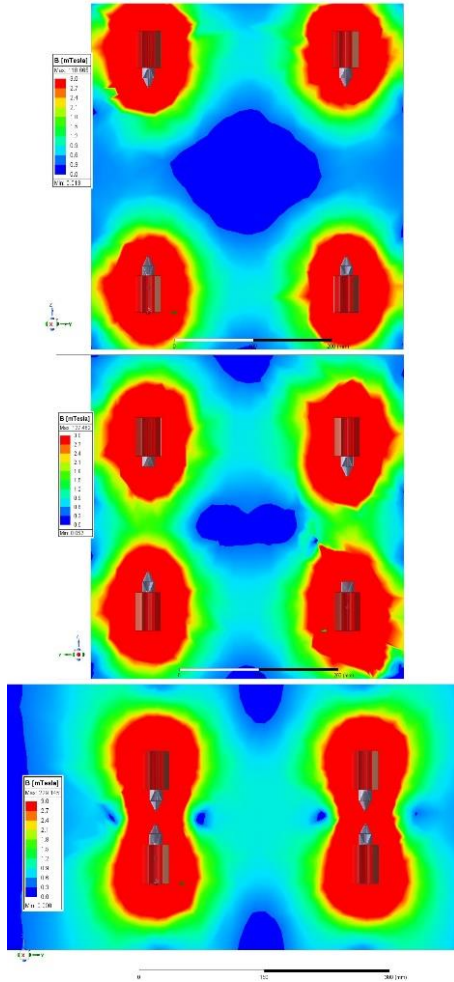**Figure 14: Alternating Polarities Configuration (Alignment Phase)**

Figure 15: The Electromagnetic Simulation of the Electromagnets with Identical Polarities Configuration

Figure 16: The Electromagnetic Simulation of the Electromagnets with Alternating Polarities Configuration

As soon the satellites reach a threshold relative distance of 20 cm, the docking controllers for both satellites will switch to the alternating polarities configuration as shown in Figure 14.

This will ensure that the disturbance torque from the geomagnetic field is minimized while performing the final docking operation and to achieve perfect alignment between the satellites. The simulation of the magnetic field generated by the eight electromagnets of the two satellites at different relative distances of 10 cm, 20 cm and 30 cm is shown in Figure 16.

To control the relative velocity of both satellites for a smooth docking operation, the docking controller on one of the satellites will actuate the electromagnets for full range of dual polarity while the other satellite will actuate the electromagnets with the same polarity.
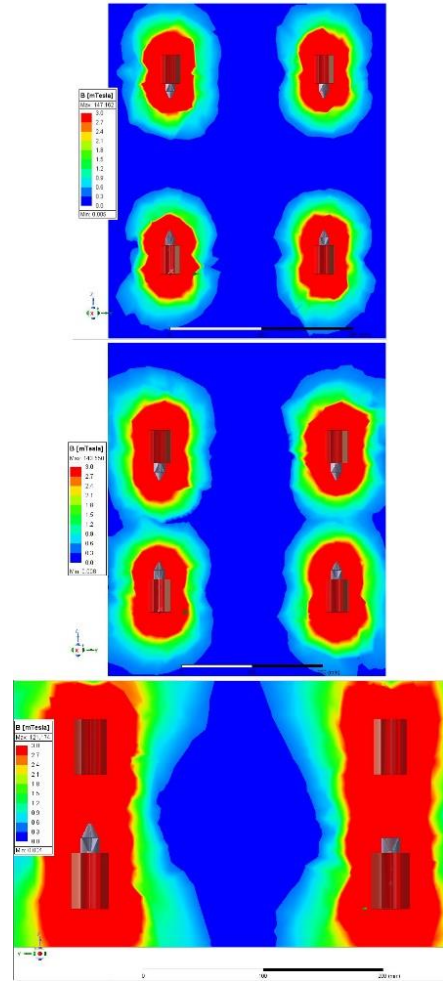
The GDC subsystem has been designed in such a way to be able to demonstrate the standardization and partial autonomy of the satellite modules. In case of a failure detected in one satellite, a Recovery and Takeover Protocol can be initiated. In this protocol, another nearby satellite can send commands to the actuators and receive sensors information directly from the recovered satellite over wireless connection.

Once failure is detected, the docking control unit will start searching for other nearby satellite's docking control unit by sending a Recovery Request message. If one nearby satellite receives the message and it has free resources to takeover, it should send back an Acknowledgement and Takeover message. As a result, a connection will be established between the new GDC subsystem and the actuators and the sensors in the recovered satellite.

Moreover, the protocol can also be initiated without a failure being identified. In this scenario, the satellite wanting to takeover will send a Takeover message directly to the other satellite. The recovered satellite should respond with an Acknowledgement message to establish the connection.

Once the two satellites docked, the resulting structure of 6U CubeSat should have the ability to move and rotate as a single unit using the two ADCSs onboard. An intelligent distributed control strategy is being developed where the actuating signal to the actuator available in the new assembled structure will adapt to certain parameters like fuel & battery remaining capacity in the corresponding satellite where the actuator is mounted and to the life expectancy of the actuator itself. As an example, when a new command is given to change the orientation of the new structure, the two ADCSs will receive the new command and activate the attitude control system but with different weighting parameters. The weighting parameters will be calculated by each ADCS independently depending on the previously mentioned parameters and on the information contained in the received Status Reports from the other satellite in the assembled structure.

THERMAL ANALYSIS

To ensure proper operation of the GDC subsystem, a thermal analysis should be performed with great care. Sensitive components such as ToF sensors, camera, UWB Modules, H-Bridges and DC-DC Buck Converter must be within the operating temperatures. Thermal analysis focuses on the distribution of temperature on the main PCB and on ensuring that the components remain within the operating temperatures. The PCB is shielded with a cover plate that protects it from space environment loads. When the docking module is activated, components like the H-Bridges and the Buck Converter generate a substantial amount of heat for their size. For this very reason, a preliminary thermal analysis was performed to estimate the maximum temperature reached during orbit. For thermal simulations, it is important to establish thermal resistance between contacting surfaces to accurately model heat flow from one surface to another. Figure 17 shows the orbit visualization of the satellite with docking side facing the Nadir and +Z axis being the velocity vector.

For the preliminary analysis, it is important to estimate the maximum temperature of the H-Bridges and the Buck Converter to simplify the simulation model as much as possible. These simplifications reduced the complexity of the thermal model and improved the simulation time for quick iterations.
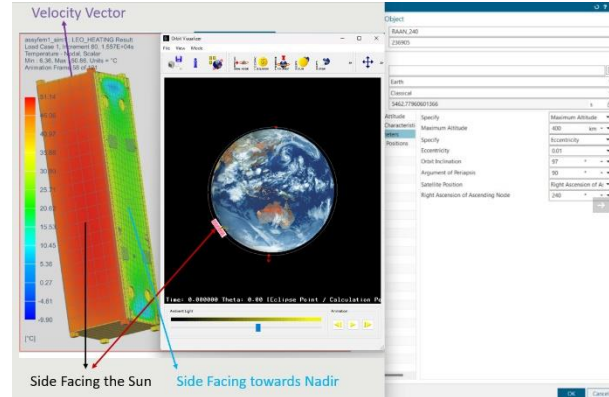

Figure 17: Orbit Visualization of the Satellite

The results from first iteration of the simulation show that the maximum temperature at the buck converter is around 400 ℃.
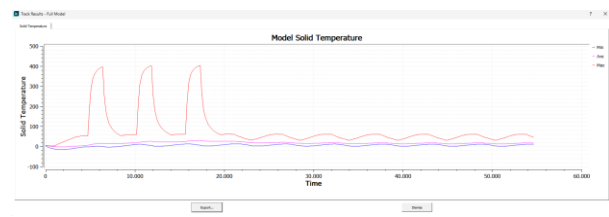

Figure 18: Maximum and Minimum Temperatures of the Model

This is because the buck converter is very small in size and dissipated large amounts of heat. This is further confirmed by Figure 19 which shows the maximum elemental temperature.
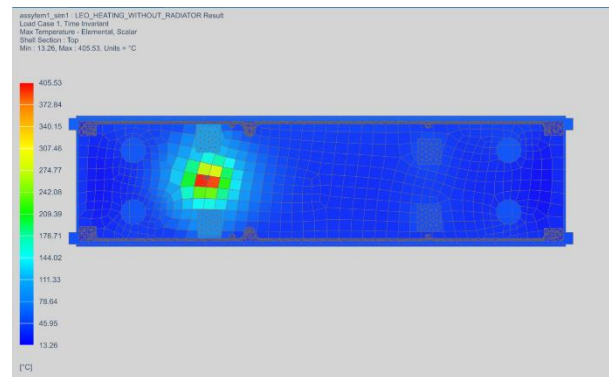

Figure 19: Maximum Elemental Temperature

The Minimum elemental temperature for the main PCB of the GDC subsystem is shown in Figure 20.

It can be shown from Figure 20 that during eclipse, the docking side stays at a temperature range of 1.8 ℃ to -8 ℃. The extreme edges reach a temperature of -16.03

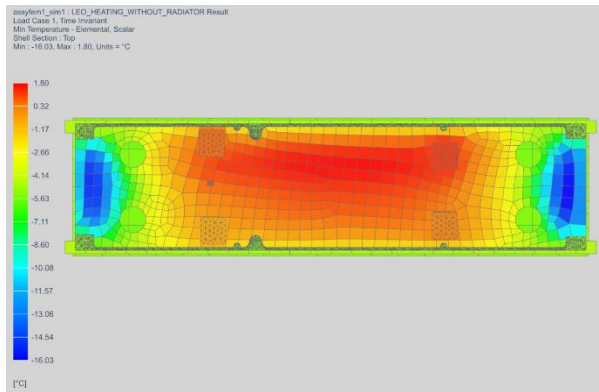°C because those regions are not shielded by the cover plate.

Figure 20: Minimum Elemental Temperature

The results from first iteration show that the temperature of the buck converter exceeds the operating temperature of -40 °C to +125 °C which is provided by the manufacturer. This is a huge problem as the buck converter will fail as soon as it is activated and will jeopardize the whole mission. To avoid this, the cover panel was modified such that it can also act as a heat sink, conducting heat from the components and radiating it to space. Figure 21 shows the modified cover plate where the grey extruded regions act as heat sinks.
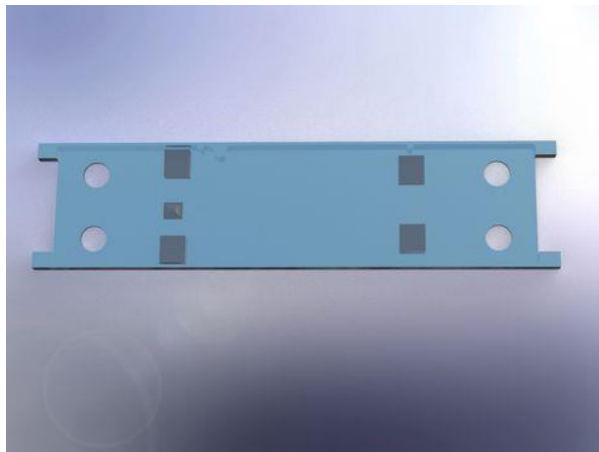

Figure 21: Modified Cover Plate with Heat Sinks

With the addition of the heat sinks, it was important to define contact thermal resistance between the top of the H-Bridges and the Buck Converter and the heat sinks.

The component layout is as shown in Figure 22. It shows how heat flows through the components to the PCB and to the heat sink, then radiating to space.
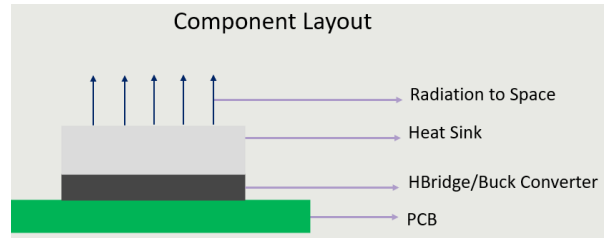

Figure 22: Heat Transfer Mode of the Component

Figure 23 shows the results of the second iteration of the simulation in which the heat sinks were added to the cover plate. The results show that the temperature of the buck converter dropped drastically from 400 °C to around 62 °C because the heat from the buck converter was conducted through the heat sink and radiated to space.
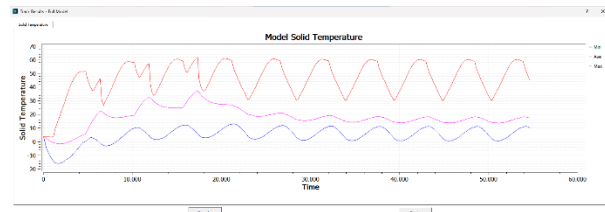

Figure 23: Maximum and Minimum Temperatures of the Model with Heat Sinks

In Figure 24, the region around the buck converter is at 62 °C. The H-Bridges reach the maximum temperature of no more than 42 °C.
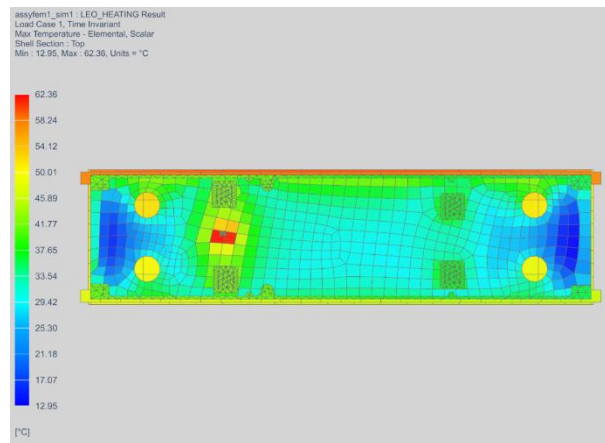

Figure 24: Maximum Elemental Temperature with Heat Sinks

Additionally, Figure 25 shows the minimum elemental temperature of the model which is in eclipse. The PCB is slightly cooler than in the first iteration without the heat sink.
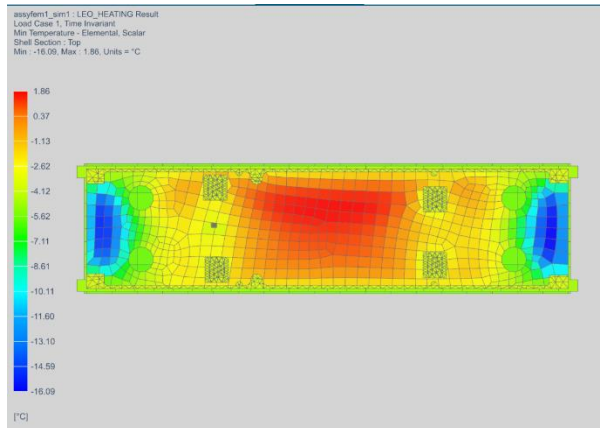
Figure 25: Minimum Elemental Temperature with Heat Sinks

The addition of the heat sinks to the cover plates has solved the heat dissipation problem for the H-bridges and the Buck Converter. However, further analysis needs to be performed for the other sensitive components in the GDC subsystem.

CONCLUSION

This paper has presented the active magnetic docking system being developed for CubeSat to perform several autonomous undocking/docking maneuvers. The mechanical and electrical designs of the docking system have been explained. Proposed designs for latching mechanism and their operations have been outlined. The guidance and docking control subsystem consisting of multistage guidance sensor systems and the docking control strategy being developed were described. An innovative proposed recovery and takeover protocol to increase system reliability and robustness has been presented. In addition, preliminary thermal analysis for the guidance and docking control subsystem has been presented and the results obtained are discussed. Further publications will be made to cover in depth the mentioned topics in this paper and show the obtained results from the developed technologies.

References

1. Redah, A., Sittner, F., Paudel, S. and S. Montenegro, "Autonomous Docking System for Assembly and Reconfiguration in Space for Small Satellites," 37th Annual Small Satellite Conference, Utah, USA, 2023.

2. Redah, A., Mikschl, T. and S. Montenegro, "Physically Distributed Control and Swarm Intelligence for Space Applications," The International Symposium on Artificial Intelligence, Robotics and Automation in Space (i-SAIRAS 2018), Madrid, Spain, 2018.

3. Kurt, H.I., Ergul, E., Yilmaz, N.F. and M. Oduncuoglu, "The Theoretical Overview of the Selected Optimization and Prediction Models Useful in the Design of Aluminum Alloys and Aluminum Matrix Composites" in Advanced Aluminium Composites and Alloys, 2020.

4. Merriam, E.G., Jones, J.E., Magleby, S.P. and L.L. Howell, "Monolithic 2 DOF Fully Compliant Space Pointing Mechanism," Mechanical Sciences, vol. 4, no. 2, 2013.

5. F. Czerwinski, "Thermal Stability of Aluminum Alloys," Materials, vol. 13, no. 15. 2020.

6. Fan, Y.Y., Gu, Y.Z., Qi, X.L., Zhang, K.H., Chen, S. and W.M. Guan, "Study on Properties of BeCu/Cu Alloy Composites," Cailiao Gongcheng/Journal of Materials Engineering, 2006.

7. Salamon, B.A. and A. Midha, "An Introduction to Mechanical Advantage in Compliant Mechanisms," Journal of Mechanical Design, vol. 120, no. 2, 1998.

8. Yunhan, H., Zhaokui, W. and Z. Yulin, "An Electromagnetic Separation System for a Spherical Satellite," in Proceedings of the International Astronautical Congress, IAC, 2020.

9. Jadhav, G.V. and S.B. Wadkar, "Analysis of Ball Lock Separation Mechanism," IOSR Journal of Engineering, vol. 02, no. 11, 2012.

10. Jones, H.M. and R.G. Daniell, "The Design and Development of a Release Mechanism for Space Shuttle Life-Science Experiments," The 18th Aerospace Mechanisms Symposium, 1984.